SCIENCE CHINA
Chemistry

• REVIEWS •
· SPECIAL ISSUE · Green Chemistry

July 2017 Vol.60 No.7: 887–903
doi: 10.1007/s11426-016-0464-1

Advances in direct production of value-added chemicals via syngas conversion

Yunlei An[1,2], Tiejun Lin[2], Fei Yu[2,3], Yanzhang Yang[2,3], Liangshu Zhong[2*], Minghong Wu[1] & Yuhan Sun[2,4*]

[1]*School of Environmental and Chemical Engineering, Shanghai University, Shanghai 200444, China*
[2]*CAS Key Laboratory of Low-Carbon Conversion Science and Engineering, Shanghai Advanced Research Institute, Chinese Academy of Sciences, Shanghai 201203, China*
[3]*University of the Chinese Academy of Sciences, Beijing 100049, China*
[4]*School of Physical Science and Technology, ShanghaiTech University, Shanghai 201203, China*

Received November 11, 2016; accepted December 27, 2016; published online April 26, 2017

Syngas conversion to fuels and chemicals is one of the most challenging subjects in the field of C1 chemistry. It is considered as an attractive alternative non-petroleum-based production route. The direct synthesis of olefins and alcohols as high value-added chemicals from syngas has drawn particular attention due to its process simplicity, low energy consumption and clean utilization of carbon resource, which conforms to the principles of green carbon science. This review describes the recent advances for the direct production of lower olefins and higher alcohols via syngas conversion. Recent progress in the development of new catalyst systems for enhanced catalytic performance is highlighted. We also give recommendations regarding major challenges for further research in syngas conversion to various chemicals.

green carbon science, syngas conversion, Fischer-Tropsh, Fischer-Tropsh to olefins, higher alcohol synthesis

Citation: An Y, Lin T, Yu F, Yang Y, Zhong L, Wu M, Sun Y. Advances in direct production of value-added chemicals via syngas conversion. *Sci China Chem*, 2017, 60: 887–903, doi: 10.1007/s11426-016-0464-1

1 Introduction

Over the past decades, considerable efforts by government, academy and industry have been directed towards providing environmentally benign products and process with high energy efficiency and low CO_2 emission. Many concepts such as "Green Chemistry", "Green Engineering" and "Green Carbon Science" and their core principles are proposed for sustainable social development [1–8]. Among these, the philosophy of green carbon sciences developed by He *et al*. [1] has received special attention in recent years. The important areas of green carbon sciences include optimization of petroleum refining, transformation of coal, methane, CO_2 and biomass. It is well-known that various fuels and chemicals are traditionally obtained from refinery of crude oil. With the rapid depletion of the limited petroleum reserves and more stringent environmental regulations, there is an urgent need for processes that can produce fuels and chemicals from alternative feedstocks [9–20]. Syngas conversion to fuels and chemicals is considered as an attractive alternative non-petroleum-based production route. The so called syngas is mainly composed of carbon monoxide (CO) and hydrogen (H_2) with different ratio and can be obtained from reforming of natural gas, gasification of coal or biomass. Many products such as ultra-clean gasoline, diesel, high quality waxes, arenes, olefins, alcohols, aldehydes, carboxylic acids, carboxylic esters, dimethyl ether can be obtained through syngas transformation.

*Corresponding authors (email: zhongls@sari.ac.cn; sunyh@sari.ac.cn)

According to the principles of green carbon sciences, one of the most effective ways is direct production of fuels and chemicals via syngas conversion [1,21,22]. Recently, direct production of lower olefins with carbon numbers range from 2 to 4 and higher alcohols with 2 or more than 2 carbons via syngas conversion has drawn special attention due to the process simplicity, low energy consumption and clean utilization of carbon resource. Major achievements in these two fields mainly involve the design of new catalyst systems for promising catalytic performance, which shows considerable potential for industrial application. Although there are still no commercial catalysts available for direct syngas conversion into lower olefins and higher alcohols, both of them are still recognized as the most challenging subjects in the C1 chemistry, and scientists keep keen interests in them. In this review, we will describe the recent progress in the direct production of lower olefins and higher alcohols via syngas conversion. The different catalyst systems for each field are outlined and discussed. In addition, the corresponding related scientific issues and requirements for future developments are also presented.

2 Direct production of lower olefins from syngas

Lower olefins, generally referring to ethylene, propylene and butylene, are basic building blocks in the chemistry industry. Ethylene, one of the largest demand chemical products worldwide, is the nucleus of the petrochemical industry. The plastics industry, with the products of polyethylene, polystyrene, polyethylene terephthalate and polyvinyl chloride, is the largest consumer of ethylene. Propylene is also an important petrochemical feedstock. Except for the production of polypropylene, propylene could be used in the synthesis of propylene oxide, cumene, acrylonitrile, isopropyl alcohol and many other industrially relevant chemicals. Butylene is an essential raw material for synthetic rubber, and is used by the fuel industry to enhance the octane number of gasoline. In the traditional petrochemical industry, ethylene is mainly produced from cracking of naphtha, petroleum gas and condensate oil [23], and propylene is the by-product of steam cracking of naphtha and fluid catalytic cracking process [24]. With the rapid growth in petroleum consumption and the limited reserve of oil sources, alternative processes are developed for the production of lower olefins [25]. Recent progress in the production of lower olefins via syngas include indirect or direct methods as showed in Figure 1 [26]. The indirect process mainly refers to the methanol to olefins (MTO or DMTO) technology [25], where an intermediate such as methanol or dimethyl ether is synthesized from syngas on copper-based catalysts and then dehydrated to form lower olefins using molecular sieve catalysts. The direct conversion of syngas into lower olefins is an interesting option compared to MTO or DMTO from the green carbon science point of view [24]. The direct routes mainly include the oxide-zeolite bifunctional catalysis process and the Fischer-Tropsch to olefins (FTO) process. The MTO or DMTO process has already been commercialized, and many reviews have discussed its development in details [27–32]. Herein, we focus on the progress in the direct production of lower olefins via syngas.

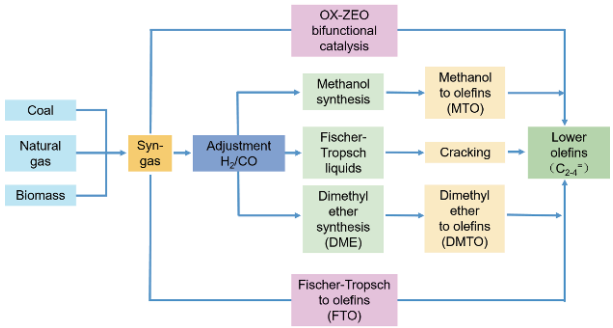

Figure 1 Different reaction paths for the production of lower olefins via syngas conversion [26] (color online).

2.1 Bifunctional catalysis route for direct production of lower olefins

In order to simplify the MTO process, scientists attempted to find a catalyst with two components to couple the methanol synthesis and the C–C coupling reaction, where one component of the catalyst is used to activate CO to form methanol or similar intermediates, and the other component, such as zeolite, is responsible for the C–C coupling for olefins formation. Due to the extremely low activity of the MTO reaction at low temperature, the methanol synthesis has to be operated at rather high temperature (ca. 400 °C). Considering the low selectivity to methanol for the traditional Cu-Zu-Al catalyst at the temperature of the MTO reaction, high temperature methanol synthesis catalysts with the composite oxides including Zn and another transition metal such as ZnCr or ZnZr, are chosen as one part of the bifunctional catalyst. However, due to the thermodynamic limitation on methanol synthesis at high temperature, it needs a rapid formation of olefins on zeolites to enhance the overall CO conversion [25,33–42].

Recently, Jiao *et al*. [43] reported an OX-ZEO catalyst system to produce olefins from syngas (Figure 2). They chose ZnCr composite oxides to activate the CO molecule, combined with meso-SAPO-34 molecular sieve to offer the acid site for olefins formation. The prepared $ZnCrO_x$/MSAPO catalyst could reach 80% selectivity of lower olefins with the CO conversion of 17% under the condition of 400 °C, 25 bar and a H_2/CO ratio of 1.5 (Figure 3). They suggested that CO and H_2 were activated to form CH_2 species on the surface of $ZnCrO_2$ with abundant oxygen vacancies after *in situ* treatment in H_2 for 2 h at 310 °C. Such CH_2 species are very active and

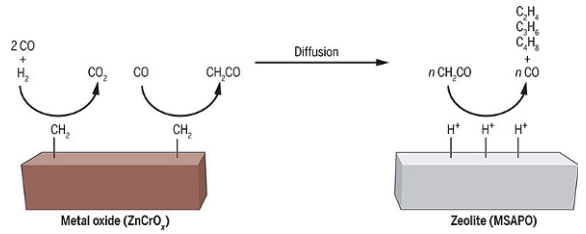

Figure 2 OX-ZEO bifunctional catalyst for direct production of olefins via syngas [42] (color online).

readily react with CO in the presence of H_2, forming a relative less reactive ketene intermediates. Compared with the traditional MTO catalyst, the bifunctional catalysts for direct synthesis of olefins from syngas have longer operation life and there was no evident deactivation after reaction for 650 h.

Almost at the same time, Cheng *et al*. [44] reported a coupling of the methanol-synthesis and methanol-to-olefins reactions with a bifunctional catalyst that can realize the direct conversion of syngas to lower olefins with an exceptionally high selectivity. Under the conditions of 400 °C, 10 bar and a H_2/CO ratio of 2, the selectivity of lower olefins reached 74% with the CO conversion of 11% (Figure 4). They suggested that CO could be activated at the oxygen vacancies of ZrO_2 surface and formed surface methoxide via formate in the presence of H_2. Due to the low ability of ZrO_2 to dissociate H_2, ZnO, which can accelerate the dissociative adsorption of H_2, was also needed. The subsequent C–C coupling proceeded on SAPO-34 molecular sieve to effectively produce C_{2-4} olefins (Figure 5). The reaction temperature of methanol synthesis was tuned to match the MTO reaction by controlling the content of Zn, and the physical mixing method was adopted to prepare the bifunctional catalyst. It was suggested that weak acid sites on the molecular sieve and proper distance of oxides and the molecular sieve facilitated the production of lower olefins.

2.2 Fischer-Tropsch to olefins

In the Fischer-Tropsch (FT) reaction, it is generally accepted that the intermediate species were formed through the cleavage of the C–O bond, and then products of different chain lengths were formed through the linking of C–C bond. The carbide mechanism for FT synthesis was firstly proposed by Fischer and Tropsch in 1926. And in the following decades, the carbide mechanism was further improved by theoretical study, dynamical modeling, isotopic tracing experiments and probe molecular techniques [45–51]. The schematic presentation of the carbide mechanism is shown in Figure 6 [51].

The direct route by Fischer-Tropsch to olefins (FTO) is another promising way to produce olefins. During the FTO reaction, the adsorbed CO molecule is first dissociated and hydrogenated to form surface CH_x monomers [45]. The carbon chain propagation is then initiated to form surface alkyl species. Further hydrogenation of the alkyl species leads to the formation of paraffins while dehydrogenation results in the production of olefins. As the reaction condition is more moderate than the OX-ZEO bifunctional route, the FTO process has attracted significant attention from both academia and industry.

In the FT reaction, the product chain growth possibility mostly follows the classical Anderson-Schulz-Flory (ASF) distribution, the mathematical expression of the ASF distribution is shown below:

$$Ln\left(\frac{W_n}{n}\right) = nLn\alpha + 2Ln\left(\frac{1-\alpha}{\sqrt{\alpha}}\right)$$

where the α represents chain growth possibility factor, and W_n represents mass fraction for the hydrocarbon with the carbon number of n. Product distribution based on ASF model is showed in Figure 7.

The process of the FTO reaction is very similar to that of typical FT synthesis, and FT catalysts can be used for production of lower olefins after suitable catalyst modification and optimization of the reaction conditions. The primary aim of FTO is to maximize lower olefins selectivity while reducing methane production. According to the ordinary ASF model, a maximum selectivity toward C_{2-4} olefins of 56.7 wt% can

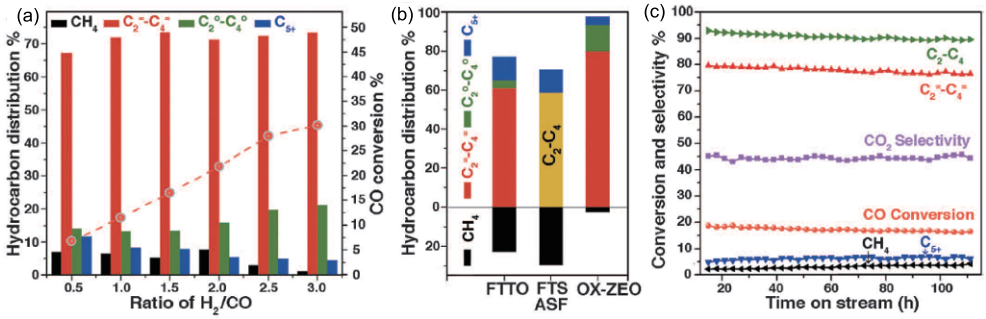

Figure 3 Catalytic performance of $ZnCrO_x$/MSAPO catalyst for lower olefins production. (a) CO conversion and product distribution versus H_2/CO ratios; (b) compare the hydrocarbon distribution among OX-ZEO, FTO and FTS that predicted by the ASF model at a chain growth probability of 0.46; (c) the stability test of $ZnCrO_x$/MSAPO catalyst [43] (color online).

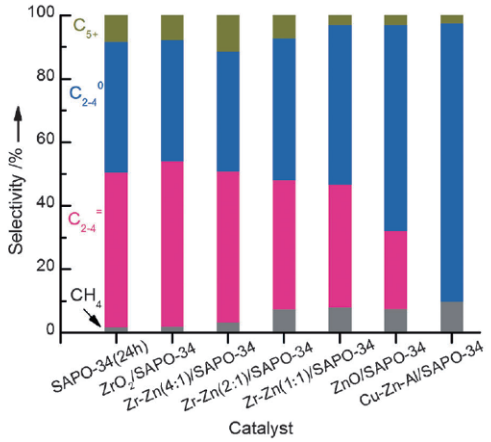

Figure 4 Comparative study of the differences in product selectivity over different catalyst systems for the conversion of methanol under H_2. Reaction conditions: 400 °C, 10 bar, 3600 mL g^{-1} h^{-1} of GSHV, 0.010 mL min^{-1}; time-on-stream (TOS)=200 min [44] (color online).

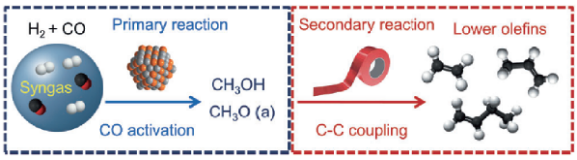

Figure 5 Reaction coupling of methanol-synthesis and methanol to olefins for direct production of lower olefins via syngas [44] (color online).

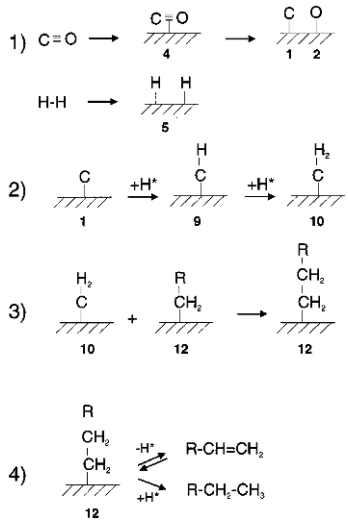

Figure 6 The carbide mechanism for Fischer-Tropsch synthesis [51].

be achieved with an α value of about 0.5 [24,51,52]. One of the most efficient ways of shifting product selectivity to low α values is by increasing the reaction temperature. However, a decrease on the chain growth probability results in an increase in methane selectivity as indicated by the ASF product distribution. In addition, the produced olefins are prone to further hydrogenation to paraffins at high temperature resulting in decreased selectivity to lower olefins. Moreover, particle sintering and coke formation at high temperature would lead to serious deactivation [53]. Due to the above limitation, there is no catalyst available for the industrial application of the direct conversion of syngas into lower olefins via the Fischer-Tropsch synthesis. Generally, most of the reported FTO catalysts are still a kind of FT catalyst with a low alpha value. The product distribution for this kind of catalysts still obeys the ordinary ASF model. Obviously, with the simultaneous goals of high selectivity to lower olefins, low methane selectivity and high stability, it is necessary to develop new FTO catalyst that deviates from the ASF distribution [24].

2.2.1 Fe-based FTO catalyst

Fe-based catalysts are widely studied for the direct production of lower olefins from syngas, and de Jong *et al.* [24] have previously reviewed these catalyst systems. In general, the Fe-based FT catalysts possess the advantages of low methanation activity, high ratio of olefin to paraffin and high water-gas-shift (WGS) activity, favorable for CO-rich syngas conversion. Some promising results have been achieved for Fe-based FTO reaction. The selectivity to lower olefins for high temperature Fe-based FT synthesis using fluidized bed can reach 24% [54]. Many research groups focused on the modification of the supports [55–61] and the effect of promoters [62–64] to maximize the lower olefins selectivity. Recently, the Fe-based catalyst promoted by S and Na and using α-alumina or carbon nanofiber as weakly interacting supports were prepared by de Jong *et al.* (61 C%) [65], and these catalysts exhibited excellent performance for selective formation of lower olefins (61 C%) as shown in Table 1.

Detailed studies on the effect of sodium and sulfur indicated that sodium was beneficial for suppressing methane formation and increasing chain growth probability values, and low loading of sulfur resulted in increasing lower olefins selectivity and catalytic activity and decreasing methane selectivity

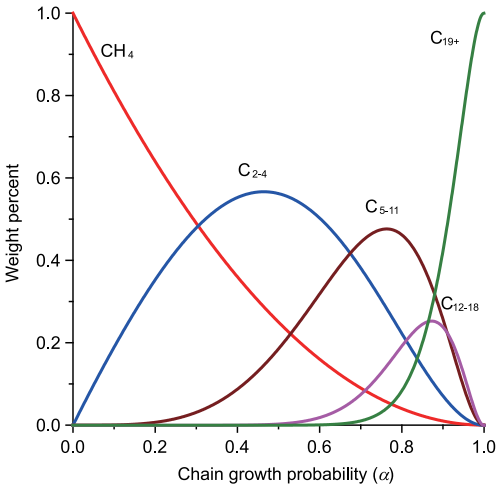

Figure 7 The typical product distribution based on Anderson-Schulz-Flory (ASF) model [26] (color online).

Table 1 The catalytic performance of different Iron catalysts [a)]

Sample	FTY [b)] (10^{-6} mol_{CO}^{-1} $g_{Fe.}$ s^{-1})	Selectivity (C%)			
		CH_4	C_{2-4} olefins	C_{2-4} Paraffins	C_{5+}
Fe/CNF	1.41	23	61	4	12
Fe/α-Al_2O_3 (12 wt% Fe)	0.65	22	61	4	13
Fe/β-SiC	6.52	31	58	4	7
Fe/SiO_2	0.14	38	56	5	1
Fe/γ-Al_2O_3	0.07	54	44	2	0
Fe-Ti-Zn-K	0.13	83	16	1	0
Fe-Cu-K-SiO_2	0.20	43	46	2	9
Bulk Fe	0.08	76	21	2	1

a) Reaction conditions: 350 °C, 1 bar, H_2/CO of 1, 20 mg of catalyst [65]; b) Iron time yield (FTY) represents moles of CO converted to hydrocarbons per gram of Fe per second.

[66]. They suggested that the effect of sulfur on the activity and product selectivity might be attributed to selective blocking of hydrogenation sites by sulfur. The author also found that the iron carbide particle size played a crucial role in the direct production of lower olefins via syngas and lower olefins are preferred to form at promoted terrace sites [67]. In addition, different ordered mesoporous materials-supported Fe-based catalysts with sulfur and sodium as promoters were investigated, as shown in Figure 8, and the carbon-supported catalysts with the weak support-catalyst interaction was found to have better FTO performance than those with strong support effect, which suppressed the formation of active iron carbide [68].

Since the Fe-based catalysts possess excellent FTO performance, the factors influencing the stability was further studied. de Jong *et al.* [69] recently reported the effect of the iron particle size and the promoter (sodium and sulfur) on the stability of Fe/CNF catalyst under the industrially relevant conditions (340 °C, 20 bar, H_2/CO=1). Their results showed that the unpromoted catalysts had lower initial catalytic activity, while the catalysts promoted with Na and S exhibited the opposite trend (Figure 9). However, substantial deactivation was observed over a period of 100 h for the promoted catalysts. The author used a tapered element oscillating microbalance (TEOM) to study the coke deposition on these two catalysts and found that the loss of active Fe surface area coincided with the increase in the Fe particle size was the main cause of deactivation.

Zhou *et al.* [70] also studied the effect of sulfur on the reactivity of catalysts by using hierarchical structured α-Al_2O_3 as support and impregnating an appropriate amount of sulfur. With the addition of sulfur, the Fe/Al_2O_3-H-8S catalyst exhibited not only enhanced Fischer-Tropsch synthesis activity and selectivity toward lower olefins, but also increased resistance against carbon deposition.

Some transition metals such as Mn, Ti and V, with higher CO affinity, are usually used as additives to improve the olefin selectivity [71–74]. Mn can play the role as both an electronic assistant and a structural promoter. On the one hand, Mn can

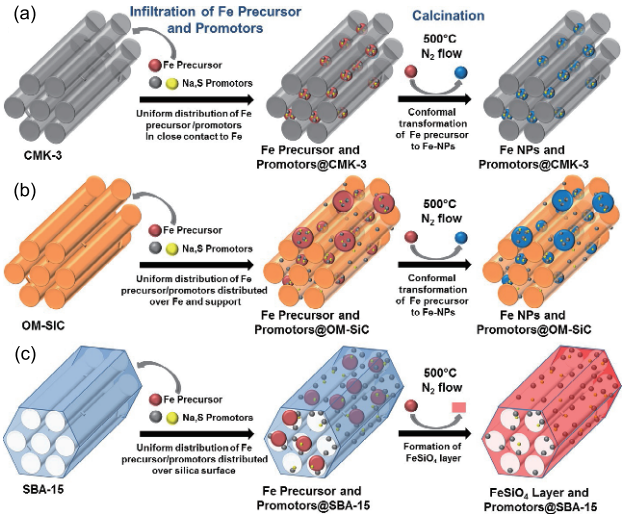

Figure 8 Schematic depiction of the preparation methods for iron supported on ordered mesoporous materials as efficient Fe-based FTO catalysts [68] (color online).

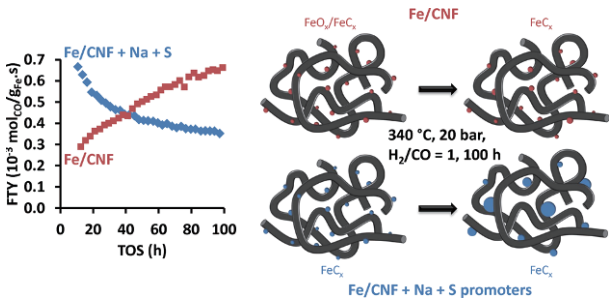

Figure 9 Size and promoter effect on stability of carbon-nanofiber-supported iron-based Fischer-Tropsch catalysts [69] (color online).

form a strong interaction with Fe to improve the dispersion of the iron species; on the other hand, it can also give some electrons to promote the dissociation of CO and improve the selectivity of olefins. Yang *et al.* [75] prepared carbon nanotube-supported Fe catalysts with different amount of K and Mn promoters. They found that Mn could increase the stability of FeC_xN_{1-x} and promote the adsorption of CO. The

study by Liu *et al.* [76] about the MnO_x modified Fe_3O_4 catalyst suggested that MnO_x nanoparticles were embedded on the surface of Fe_3O_4 microspheres (Figure 10). The Mn additive could effectively adjust the surface properties of iron carbide, inhibit olefin secondary hydrogenation reactions and improve the selectivity to lower olefins (60.1%). The X-ray absorption fine structure (XAFS) result showed that Mn could promote the formation of the θ-Fe_3C phase, which can help to improve the olefin/paraffin ratio and promote lower olefin production. The results of DFT simulations showed that H_2 could easily dissociate into adsorbed atoms at the Fe–C bond on the Fe_3C surface leading to the formation of CH_2 species by combining with absorbed C atom. The weak hydrogenation ability of Fe_3C help to improve the olefin/paraffin ratio [77].

The preparation method has much effect on the catalytic performance of Fe-based catalysts. Gao *et al.* [78] studied the FTO reaction over Zn promoted Fe-based catalyst. The addition of the Zn promoter was shown to improve both the lower olefin selectivity and the catalyst stability. Severe carbon deposition and deactivation were found to occur with the catalysts prepared via the impregnation method, which contain greater quantities of surface ZnO on the surface. However, those samples synthesized using the microwave-hydrothermal approach showed improved dispersion of Zn and Fe species, and higher activity and better stability resulting from reduced carbon deposition were thus achieved. A series of novel FeK-OX composite catalysts were reported by Duan *et al.* [79] to exhibit high selectivity to lower olefins with high stability. The method for introducing promoters and iron species was found to have a great influence on the design and fabrication of highly active, selective and stable iron-based composite catalysts for the FTO reaction.

Carbonaceous materials, such as carbon black [73], carbon nanotube [75,80,81], activated carbon [65,66,82–84] and grapheme [85], are interesting alternatives for the preparation of supported catalysts. Venter *et al.* [73] reported the highly dispersed FeMn bimetallic particles supported on a high surface area amorphous carbon black to have the lower olefins selectivity up to 76% under the reaction conditions of 275–290 °C, 1 bar and a H_2/CO ratio of 3. However, the catalytic activity decreased to 55% after 100 h of reaction in the stability test. The deactivation was suggested to be caused by the heavy carbon deposition. Carbon materials are always modified by nitrogen and oxygen doping, which could work as promoters and evidently promote the production of unsaturated hydrocarbons. Lu *et al.* [86] prepared a Fe/NCNTs catalyst using the anchoring effect and the intrinsic basicity of nitrogen-doped carbon nanotubes (NCNTs), where iron nanoparticles were conveniently immobilized on NCNTs without surface pre-modification. The obtained catalyst presented promising catalytic performance in the FTO reaction with 46.7% selectivity to lower olefins, 14.4% CO conversion as well as high stability. They suggested that the intrinsic basicity of the NCNTs support would enhance CO dissociative adsorption and promote the lower olefin desorption, resulting in high selectivity to lower olefins. The participation of the nitrogen is responsible for the high activity as it can promote the reduction of iron oxide and accelerate the formation of the active χ-Fe_5C_2 phase (Figure 11).

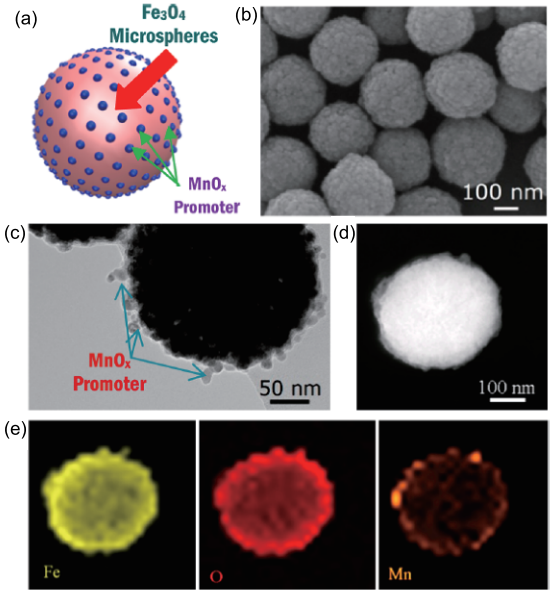

Figure 10 (a) Structural model for the Mn/Fe_3O_4 catalyst; (b) scanning electron microscope (SEM) images of the Fe_3O_4 microspheres; (c) transmission electron microscope (TEM) images of the reduced 6 wt% Mn/Fe_3O_4 catalyst; (d) original scanning transmission electron microscopy (STEM) image of the 6 wt% Mn/Fe_3O_4 catalyst as prepared; (e) the corresponding STEM-energy dispersive X-ray spectroscopy (EDX) elemental mapping of Fe, O and Mn on the catalyst [76] (color online).

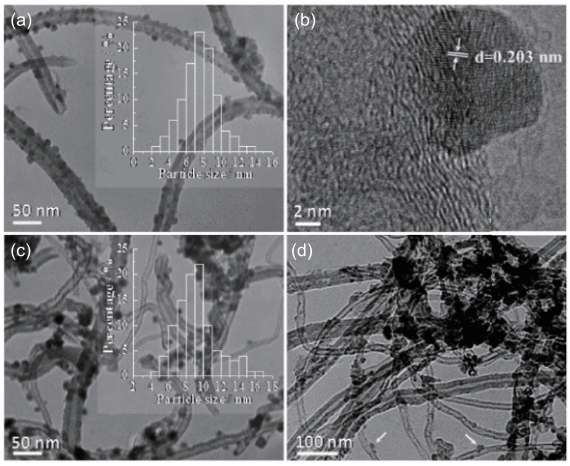

Figure 11 TEM and high resolution TEM (HRTEM) characterization of activated catalysts with iron loading of 10 wt%. (a, b) Fe/NCNTs; (c) Fe/t-CNTs; (d) Fe/u-CNTs. The insets in (a) and (c) are the corresponding particle size distributions [86] (color online).

A supported iron-based catalyst using the nitrogen and oxygen functionalization of CNTs as the support was prepared by Schulte *et al*. [56]. The sample was then tested under the industrially relevant conditions of 340 °C, 25 bar and a H_2/CO ratio of 1. The catalyst was shown to have comparable initial conversion with an excellent olefin selectivity [$S(C_{3-6})$>85%] and a low chain growth probability (a≤0.5). Nitrogen- and oxygen-containing functional groups were found to act as efficient anchoring sites for the deposited iron nanoparticles.

N-doped graphene is also an efficient electron donor to iron catalysts for CO hydrogenation. A supported iron catalyst with N-doped graphene prepared by Chen *et al*. [85] showed high selectivity to lower olefins of ca. 50% under the conditions of 340 °C, 5 bar and a gas hourly space velocity (GHSV) of 5000 h^{-1}. The X-ray absorption spectroscopy (XAS) result of the Fe L-edge and X-ray diffraction (XRD) indicated that the iron supported on N-doped graphene possessed a more reduced state, which could promote the selectivity of light olefins.

Long chain olefins are also important platform chemicals for producing highly valuable products, such as aromatic compounds and lubricating oils, as well as higher alcohols [87]. Zhai *et al*. [88] fabricated Zn- and Na-modulated Fe catalysts by a simple co-precipitation/washing method. Zn was found to serve as a structural promoter, and the existence of Na on the surface of the Fe catalyst altered the electronic structure, making the catalyst very active for CO activation. In addition, the electronic structure renders the catalyst unexpectedly selective toward olefins—especially C_{5+} olefins (with more than 50% selectivity in hydrocarbons)—while lowering the selectivity of undesired products (Figure 12).

2.2.2 Co-based FTO catalyst

For the CO hydrogenation reaction, cobalt (Co) is also an effective active metal for application in the industrial FTS process. Compared with iron, cobalt has long been considered the most favorable metal for the synthesis of long chain hydrocarbons due to its high activity, high selectivity to linear paraffins, and low water-gas shift (WGS) activity [52,89], thus the Co-based catalysts generally believed to be not suitable for production of shorter chain hydrocarbons and olefins. However, Dan *et al*. [90] reported a Co^0-CdA catalyst prepared using Cd vapors as the reducing agent to reduce CoY (Co^{2+} ions exchanged into A-type zeolites), and propylene was found to be the only detectable hydrocarbon product at the conditions of 151 °C, 6.5 bar and a H_2/CO ratio of 1. However, the Co clusters in the cage were unstable, easily migrated to the outside of the cage, and agglomerated to large particles during the reaction. Mirzaei *et al*. [91] prepared cobalt manganese oxides by co-precipitation and studied them for the conversion of syngas to lower olefins. The effect of a range of preparation variables was investigated in great details. They found the CoMn catalyst with an appropriate support to possess the lower olefins selectivity up to 50% at 450 °C. In addition, other Co-based catalysts have also been reported for the FTO production [92–94].

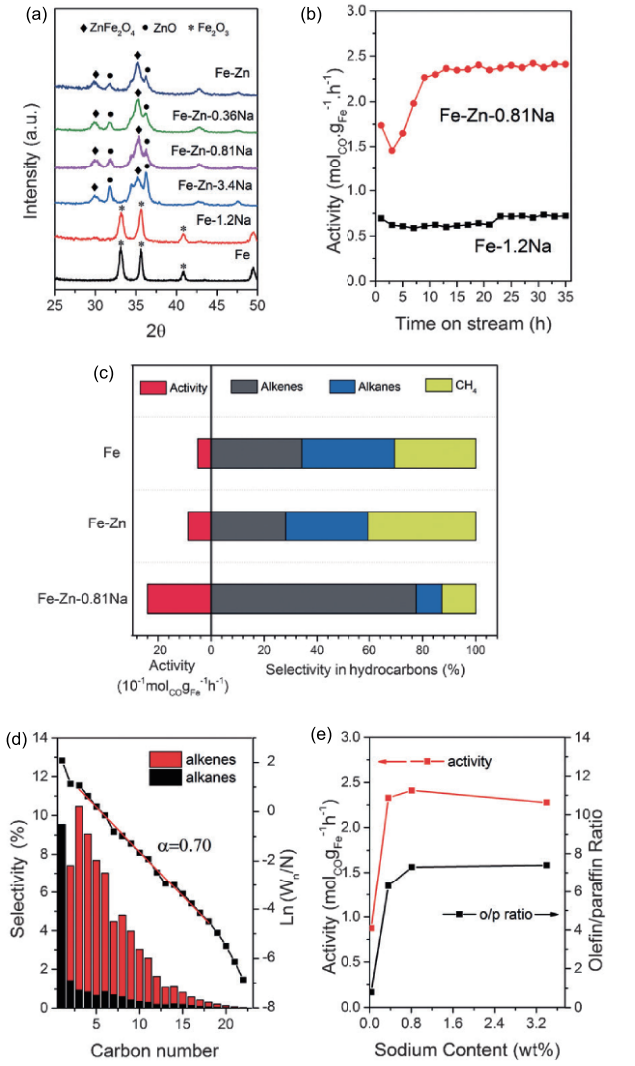

Figure 12 (a) XRD patterns of the calcined catalysts; (b) the comparison of activity vs. TOS between Fe-Zn-0.81Na and Fe-1.2Na catalysts; (c) the activity and product distribution over Fe-Zn-0.81Na, Fe-Zn, and Fe catalysts (reaction conditions: 340 °C, 20 bar, syngas ($CO:H_2:CO_2:Ar$=24:64:8:4), 60000 mL g^{-1} h^{-1}); (d) the hydrocarbon distribution and Anderson-Schulz-Flory (ASF) plot over Fe-Zn-0.81Na; (e) catalytic activity and the *o*/*p* ratio as a function of Na content [88] (color online).

Recently, our group [95] discovered the cobalt carbide (Co_2C) quadrangular nanoprism catalyst, which was obtained after the reaction using a cobalt-manganese complex oxide ($Co_xMn_{3-x}O_4$) catalyst, to exhibit high selectivity to lower olefins (~60.8 C%) as well as low selectivity to methane (~5.0 C%) at the conditions of 250 °C, 1 bar, a H_2/CO ratio of 2. The product distribution deviated greatly from the classical ASF distribution with the ratio of olefin to paraffin (O/P) for the C_{2-4} slate to be as high as 30. Decreasing the H_2/CO ration from 2 to 0.5 greatly improved the O/P ratio for

the C_{2-4} slate to 51, making it suitable for the H_2-lean syngas conversion. We were astonished to find the CO-conversion rate and the product selectivity to change considerably with time on stream. At the first 4 h of reaction, the activity gradually decreased to a minimum value of 6.8% and then increased continuously at the expense of C_{5+} selectivity over the next stage. The selectivity to lower olefins, methane and CO_2 increased first with time-on-stream and then remained stable. To elucidate the catalyst structure evolution, we carried out in-depth studies using XRD and TEM characterization, and found the Co_2C to play a vital role in the lower olefins formation. With TOS of reaction ranged from 0 h to 150 h, the content of Co_2C increased from 10.3 wt% to 50.6 wt%, while metallic Co with mass percentage of 3.9 wt% only existed at the initial reaction stage. Formation of Co_2C was traditionally regarded as the main cause of deactivation during the FT reaction with low activity and high methane selectivity, the Co_2C nanoprisms obtained in our experiments must be different from the reported Co_2C phase. Detailed studies suggested that the residual sodium in the as-prepared CoMn catalyst enhanced the formation of Co_2C while the manganese contributed to the formation of nanoprisms, via the $Co_xMn_{1-x}O$ precursor. Precise characterization of the surface structure of the Co_2C catalyst revealed a strong facet effect for Co_2C nanoparticles during syngas conversion. More specifically, the (101) and (020) facets of Co_2C are beneficial for the production of olefins and inhibit the formation of methane (Figure 13). Further DFT calculations demonstrated that the CH_2CH_2 species remain the most stable on the Co_2C (101) surface, and methane is difficult to form on both Co_2C (101) and (020), which agree well with the experimental finding. The stability test of more than 600 h was carried out over this CoMn catalyst from an industrial viewpoint as showed in Figure 14, and no obvious deactivation was observed, indicating the promising potential for industrial applications. Claeys [96] claimed that this findings may provide new ideas and pathways on the Co-based catalysts as well as other forms of carbides for this reaction.

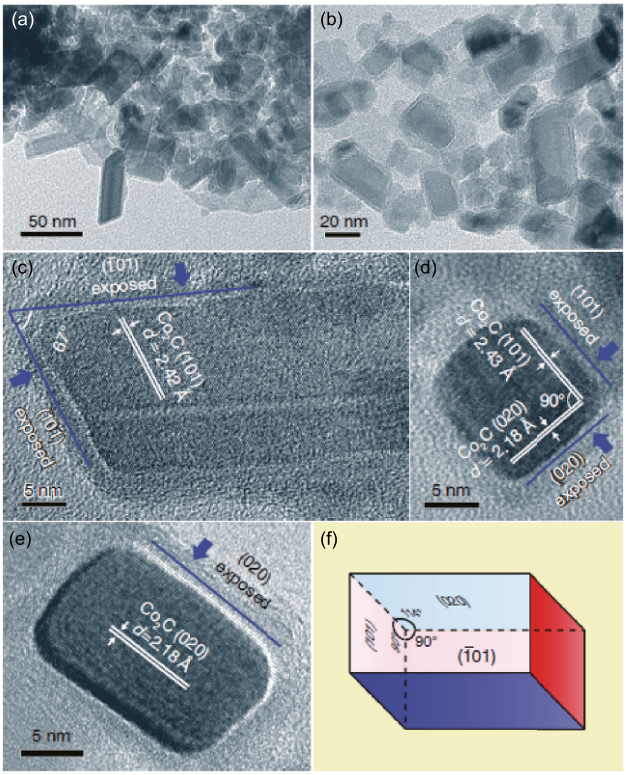

Figure 13 TEM characterization of the CoMn catalysts at the steady stage of reaction. (a, b) Low-resolution TEM images; (c, e) high-resolution images of Co_2C nanoprisms with exposed facets of (101), (−101) and (020); (d) distance (length) of the lattice fringes; (f) the Co_2C nanoprisms model with four rectangular faces and two rhomboid faces [95] (color online).

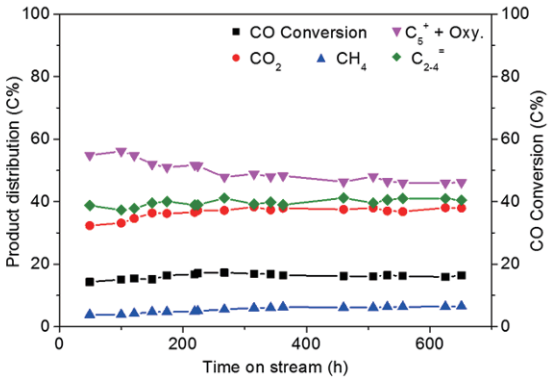

Figure 14 The stability test of CoMn. Reaction conditions: 250 °C, 3 bar, 6000 mL g^{-1} h^{-1} and H_2/CO of 1 [95] (color online).

3 Higher alcohol synthesis

Higher alcohols, which commonly refer to alcohols with carbon number higher than that of methanol, are widely used in many applications. For example, C_{2-5} higher alcohols mixed with methanol could be used as fuels and fuel additives for octane enhancement and C_{6+} alcohols could be used as valuable feedstocks for detergents, plasticizers and lubricants [97,98]. With increasing environmental concerns, energy security issues and strong desire for greener processes, higher alcohol synthesis (HAS) via syngas conversion continues to gain considerable attention [1,97].

The reaction pathway for HAS is very complicated, and concerns many reaction process such as Fischer-Tropsch synthesis and the water-gas-shift reaction. There are generally multiple products including alcohols, paraffins, olefins, and other chemicals present in the catalytic conversion of syngas. Some important reactions are listed as follows:

$$n\mathrm{CO} + 2n\mathrm{H_2} = \mathrm{C_nH_{2n+1}OH} + (n-1)\mathrm{H_2O} \quad (1)$$

$$n\mathrm{CO} + (2n+1)\mathrm{H_2} = \mathrm{C_nH_{2n+2}} + n\mathrm{H_2O} \quad (2)$$

$$CO + H_2O = CO_2 + H_2 \quad (3)$$

Among them, Reaction (1) is the higher alcohol formation reaction; Reaction (2) is the typical FT reaction while Reaction (3) is the water-gas-shift reaction [99].

Much work has been done on higher alcohol synthesis around the world in the aim of improving the catalytic performance including the catalytic activity, alcohol selectivity and stability. Different reaction mechanisms and active sites were reported over different catalyst systems. Generally, there are four types of HAS catalysts: modified methanol catalysts, modified Fischer-Tropsch (FT) catalysts, molybdenum based catalysts, and rhodium based catalysts. The modified methanol catalysts, developed by Snam in Italy and Lurgi in Germany, include the high pressure (HP) and low pressure (LP) types. The main alcohols obtained are methanol and *iso*-butanol [100–103]. Modified FT catalysts mainly include Fe-based and Co-based catalysts [99,104,105], which feature high selectivity to higher alcohols. The products generally obey the Anderson-Schulz-Flory (ASF) distribution [106]. Molybdenum-based catalysts represent molybdenum oxide-, molybdenum sulfide-, and molybdenum carbide-based catalysts. The main products of molybdenum based catalysts are C_{1-5} straight chain primary alcohols [107]. Although Rhodium-based catalysts show the best selectivity to C_{2+} oxygenates than other catalyst systems, the high price and limited availability hinder their industrial applications. Except for the Rh-based catalysts, the other three still suffer from low selectivity to alcohols, particularly to higher alcohols, and poor stability. Therefore, novel catalysts suitable for HAS with high selectivity and stability are highly desired.

The modified FT catalysts have been studied over decades due to their attracting product distribution. There have been a lot of reports in the literature on the reaction mechanism, catalyst systems, kinetics and process engineering of modified FT catalysts for HAS [97,99,105,108]. And it is also well recognized that dual sites with different functions are needed for modified FT catalysts. One active site such as Co^0 or FeC_x serves for CO dissociation, carbon chain growth and hydrocarbon formation, and the other active site for the non-dissociative insertion of CO, for example Cu or Co_2C. The exact nature of the actual active dual sites is still unclear, and recent works focus on the optimization of catalyst preparation and reaction conditions, while some work discussed the effect of the promoters and the elucidation of the active site through the combination of experimental and DFT studies. The establishment of the stronger synergism effect between the dual sites is one of the significant recent progress. Herein, some typical results for HAS over the modified FT catalysts are presented and discussed.

3.1 Reaction mechanism

In our previous review [105], the reaction path and mechanism over the modified FT catalysts were discussed in details. Generally, the CO insertion mechanism proposed by Xu *et al*. [106] (Scheme 1) is widely accepted, which includes the FTS process and methanol synthesis process. In this mechanism, similar to the FT reaction, CO dissociates (k_d, k_1) and propagates (k_p) to form surface alkyl species (C_nH_z*), which are further transformed into different products based on the termination reaction of the alkyl species. Termination by CO insertion (k_{CO}) gives surface acyl species (C_nH_zCO*) which is then hydrogenated to alcohols (k_H'). Termination by dehydrogenation or hydrogenation (k_H) gives olefins and paraffins, respectively. During HAS, there is always competition between alcohol formation and hydrocarbon formation. The CO insertion mechanism can explain the experimental observations that the modified FT catalysts mainly produce linear primary alcohols and that alcohols obey the ASF distribution with a chain growth factor similar to hydrocarbons.

Although the CO insertion mechanism gives the detailed reaction routes of the surface species, the detailed structure of the dual sites on modified FT catalysts is still unclear. For the Cu-modified FT catalysts, many researchers tend to believe in a Cu–M structure proposed by Xu *et al*. for HAS. The M refers to the FT element (Fe, Co, etc.). On the Cu–M dual sites, CO dissociates on the FT element (Fe, Co, etc.) and converts into methylene species by hydrogenation, thus initiating the chain growth to form surface alkyl species. And CO adsorbs molecularly on Cu and inserts into the alkyl–metal bond to form acyl species (C_nH_zCO*). As depicted in Scheme 2, molecularly adsorbed CO on Cu and surface alkyl group on the FT element can combine to give surface acyl either by migration of either molecularly adsorbed CO or surface alkyl group to the FT element or Cu, respectively. Hydrogenation of the surface acyl groups gives alcohols. Both routes require the synergism between the Cu and FT elements and loss of this synergism will decrease the alcohol selectivity.

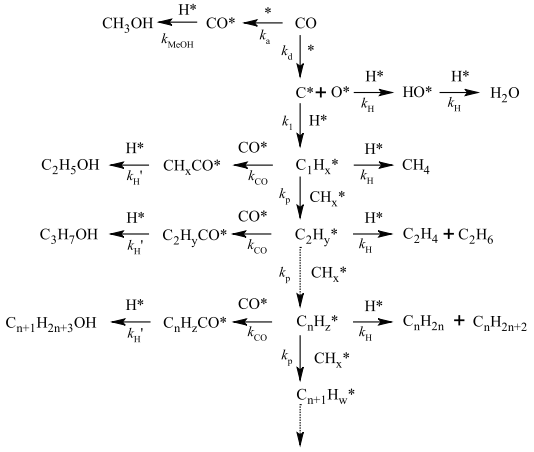

Scheme 1 CO insertion mechanism over modified FT catalysts [106].

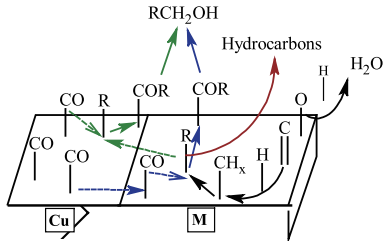

Scheme 2 Schematic depiction of the Cu-M dual sites for high alcohol synthesis [105] (color online).

3.2 Modified Co-based catalysts

The Co-based catalysts are the most studied systems for HAS. Among them, the Cu modified Co-based catalysts are especially well-known. Since the IFP developed the Cu-Co catalysts in the 1980s, these catalyst systems received much attention due to their high total alcohol selectivity and high C_{2+} alcohol distribution. According to the theory of the dual sites, many groups attempted to design Cu-Co catalysts with intimate contact in order to improve the catalytic performance and prevent the Cu phase segregation. The Cu-Co alloy and Co@Cu or Cu@Co core shell nanoparticles were usually prepared with different preparation methods. The catalytic performance, kinetics and deactivation behavior were investigated. Electronic and structure promoters were also incorporated into the catalyst systems to stablize the special dual site structure and improve the higher alcohol selectivity [109–114].

Prieto *et al*. [115] performed DFT calculations and microkinetic modeling to predict the preferred metal sites and the optimal composition. According to their prediction, they carried out the controlled synthesis of the superior Cu-Co alloy catalysts for the selective conversion of syngas to higher alcohols. The so-called precise synthesis methods were based on metal nanoparticle exsolution from a molybdate precursor compound whose crystalline structure isomorphically accommodates Cu^{2+} and Co^{2+} cations in a wide range of compositions. A Cu/(Cu+Co)ratio of 0.35 was found to give the maximum selectivity to ethanol and higher alcohols, which were close to 50 C% and 60 C%, respectively. Meanwhile, the maximum yield of C_{2+} alcohols with 27 mmol g_{Cu+Co}^{-1} h^{-1} was achieved.

In other reports, catalysts such as $CuCoO_2$ [116], $CuCo_2O_4$ [117], $LaCo_{1-x}Cu_xO_3$ [118,119] and CuCoAl-LDH [120], were used as the precursors to facilitate the formation of Cu-Co alloys. The deactivation of these Cu-Co alloy catalysts was also investigated. Liu's group [110] claimed that the deactivation of the Cu-Co alloy catalyst was mainly due to volatilization of cobalt species, whereas sintering and coke deposition were hardly observed. Co_2C might play a protective role for the decomposition of the Cu-Co alloy and volatilization of cobalt species. However, Yang *et al*. [121] prepared a Cu-Co model catalysts by the deposition-precipitation method and found an obvious structural evolution of catalysts during the reaction. They observed severe sintering of the catalyst and the formation of Co_xC on the catalyst surface, both of which reduced the number of surface Co atoms and led to catalytic deactivation.

It is commonly accepted that the Cu phase is easy to ensemble on the catalyst surface due to its lower surface energy than Co atoms, and cover surface Co atoms. To illuminate the role of Cu in the Cu-Co alloy catalyst, Su *et al*. [122] performed the kinetic studies and investigated its dynamic structure. They drew the conclusion that the addition of Cu will weaken the CO/HCO dissociation, reduce the formation of CH_x species, control surface Co ensemble size and inhibit CH_x insertion.

Besides metallic alloys, Kruse's group [123–126] developed the core shell structure catalysts for HAS. They used the oxalate route for the catalyst preparation. Typically, co-precipitation of metal salts with oxalic acid as the precipitant was adopted to produce the oxalate precursors and then perform the thermal decomposition to prepare "CoCuMn" [123,125] (Figure 15) and "CoCuNb" [126] (Figure 16) nanosized core-shell particles. The CoCuMn catalysts usually showed selectivities to 1-alcohols or combined 1-alcohols/1-alkenes higher than 60% and occasionally up to 95%. The product distribution obeys the Anderson-Schulz-Flory distribution. Because the calculated chain-lengthening probabilities for these products are higher than 0.6, but usually below 0.9, these catalysts were suggested to be good candidates for producing the C_{8-14} slate as feedstocks for plasticizers, lubricants, or detergents. For the "CoCuNb" ternary catalyst, a bimodal nanosized particle structure was obtained by oxalate co-precipitation. The bimodal nanosized particle distribution contained Co-Cu particles with sizes ranging from 25 nm to 40 nm, which plays the role of CO dissociation and CO insertion, and smaller Nb oxide particles (mainly NbO_2) between 4 and 8 nm in size, which play the role of the structural dispersant ("spacer") and the promoter for 1-alcohol/1-olefin production. The selectivities to 1-alcohols with mainly the C_{2-5} slate usually exceeded 50 wt%, and the combined selectivities to 1-alcohols/1-alkenes were 73 wt% for CO conversions ranging between 5% and 20%. Different from the ternary metal catalysts, a CuCo bimetallic model catalyst was also prepared by this group, as shown in Figure 17 [124]. The influence of the precursor activation was investigated. Significant restructuring was found to occur during precursor activation, which would further affect the catalytic performance. This study showed that the reduction conditions have a great influence on the structure of the active site. To design a highly efficient HAS catalyst, each step should be precisely controlled.

Dong *et al*. [127] developed a cobalt-copper catalyst promoted by "herringbone-type" multiwalled carbon nanotubes (CNTs). This catalyst displayed a high (C_{2-8}-alc.+DME)-

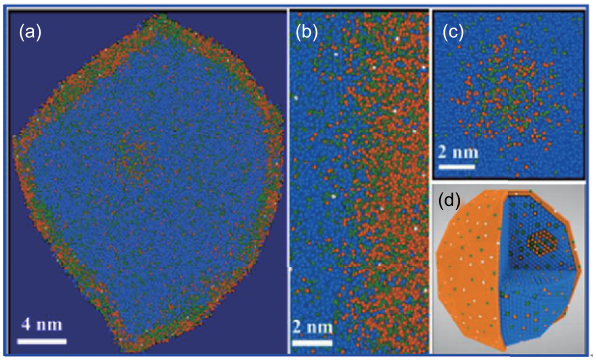

Figure 15 3D tomographic reconstructions of atom probe microscopy results for a CoCuMn core-shell nanoparticle. (a) Atom map result of CoCuMn catalyst nanoparticles; (b, c) an enlarged view from a 5 nm thick slice of the particles at the core-shell interface and intracore; (d) a 3D model of the core-shell nanoparticles [125] (color online).

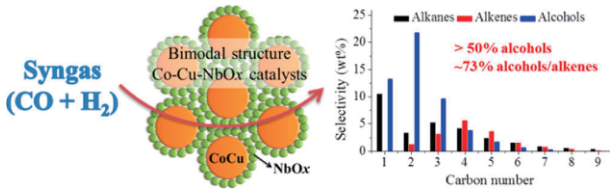

Figure 16 Ternary cobalt-copper-niobium catalysts for the selective CO hydrogenation to higher alcohols [126] (color online).

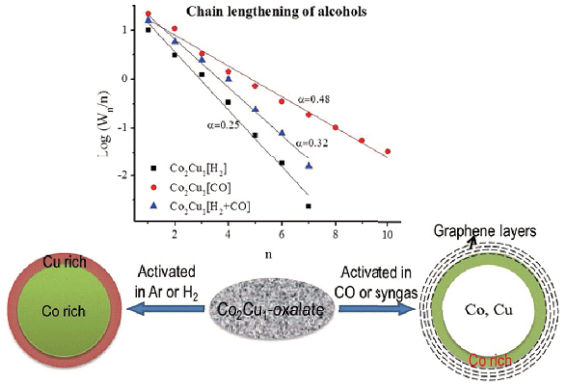

Figure 17 Influence of precursor activation on structure and HAS performance for CuCo catalyst [124] (color online).

STY of 760 mg g^{-1} h^{-1} under the reaction conditions of 50 bar and 300 °C, which was 1.78 times that of the CNT-free host, Co_3Cu_1. They ascribed the considerably increased yield of alcohols to: (1) an increase of the concentration of CoO(OH), responsible for the selective formation of higher alcohols; (2) excellent adsorption performance for H_2 with this kind of CNTs; (3) synergism of the high surface-concentration H-adspecies with CO_2 in the feed-gas.

Gao *et al.* [120] demonstrated the fabrication of core-shell Cu@(CuCo-alloy) nanoparticles (NPs) embedded on an Al_2O_3 matrix via an *in situ* growth of CuCoAl-LDH nanoplatelets on aluminum substrates followed by a calcination-reduction process, whereby the composition, particle size and shell thickness could be tuned by changing the Cu/Co molar ratio in the LDH precursors. When serving as efficient catalysts toward CO hydrogenation to produce higher alcohols, the catalyst with a Cu/Co ratio of 0.5 showed the best catalytic performance with a CO conversion rate of 21.5% and a selectivity (C_{6+} 1-alcohols slate) of 48.9%. The unique electronic and geometric interaction between Cu and Co in the Cu@(CuCo-alloy) NPs, which avoids the phase separation, contributed to the significantly enhanced catalytic performances. In addition, the open channels associated with the 3D hierarchical structure of the Cu@(CuCo-alloy)/Al_2O_3 catalyst facilitated mass diffusion/transportation as well as prevented hotspot formation, thus increased its stability and recyclability.

Although copper was traditionally believed necessary for modify Co-based catalysts for HAS, a lot of evidences have shown that Co^+/Co could also be the active site for HAS, where cobalt species with higher valance could adsorb CO non-dissociatively. The recently published Co-based HAS catalyst systems without the addition of Cu mainly include CoGa [128], CoMn [129], Fe-promoted Co/AC [130,131], etc. The typically active dual sites in these catalysts are the Co-Co_2C model. There is no doubt that Co_2C formed during the FTS is responsible for its deactivation. However, the formation of Co_2C has positive effect on the oxygenate production [132].

Ding's group [130,131,133–135] prepared a series of Co-based catalysts without Cu, and it was found that the formation of the Co and Co_2C interface and the dual sites at the interface would be essential for highly efficient alcohol synthesis via the FT reaction (Figure 18). The noble-metal-like Co_2C serves as the CO nondissociative adsorption, and the metallic Co works as the CO dissociative adsorption and subsequent carbon-chain propagation.

In order to produce more Co_2C and improve the catalytic performance, promoters such as alkali [136], La_2O_3 [98], CaO

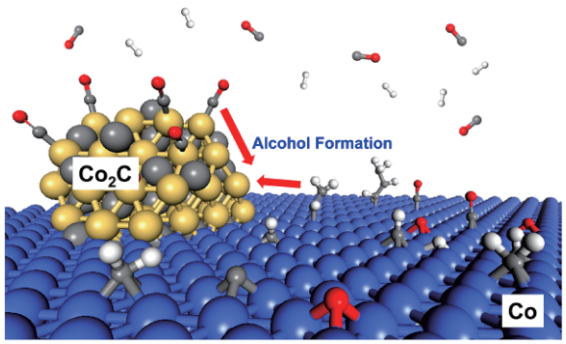

Figure 18 Schematic depiction of the formation of high alcohols via syngas conversion at cobalt metal/carbide interface [135] (color online).

[137], Al_2O_3 [138], SiO_2 [139], activated carbon [135], ZrO_2 [140], and ZnO [141] were added to Co-based catalysts. Anton *et al*. [142] studied the effect of sodium on the structure-activity relationship of cobalt-modified $Cu/ZnO/Al_2O_3$ catalysts for HAS, and they found that the presence of Na facilitated the carbidization of Co metal sites to form bulk Co_2C. A close contact between metallic Co^0 and Co_2C was assumed to generate additional active site for HAS.

Spivey's group [143,144] investigated the CuCo and La-modified CuCo catalysts and found that Cu was unable to adsorb CO associatively at the reaction temperature for HAS by DRIFTS. They therefore believed that Cu could not be involved in the CO insertion step and the effect of Cu was to provide hydrogen via H_2 spillover to hydrogenate the intermediates. The Co_2C formed on the Co^0 site can associatively adsorb CO and insert it into the adjacent CH_2 species. Thus, the Co-Co_2C constitutes the dual active sites.

Recently, Xiang *et al*. [145] found CoMn catalysts could be tuned to produce long-chain *n*-aldehydes, 1-alcohols and olefins, as well as *n*-paraffins, and the sum selectivity of aldehydes and alcohols was usually 45 wt% where up to 97% could be *n*-aldehydes. Besides, they advocated a synergistic interaction between a Mn_5O_8 oxide and a bulk Co_2C phase (Figure 19), promoted by the presence of potassium, to be responsible for the unique product spectra in their studies. The physicochemical characterization of potassium promoted CoMn catalysts revealed the occurrence of a potassium-Mn_2(II)Mn_3(IV)O_8 phase (both before and after reaction). Both phases seemed to be in intimate contact during the synthesis and were anticipated to act synergistically to produce straight-chain oxygenates (*n*-aldehydes and terminal *n*-alcohols), α-olefins and *n*-paraffins with selectivities depending strongly on the H_2/CO partial pressure. Summing C_{4+} oxygenates and hydrocarbons for each C_n, a chain-lengthening probability independent of the H_2 partial pressure was obtained. This would appear to be in agreement with a unique chain-lengthening mechanism for all product classes. A definitive proof cannot yet be provided on the basis of steady-state kinetic experiments, which would require extensive spectroscopic and microscopic in operando investigations as performed in a number of laboratories.

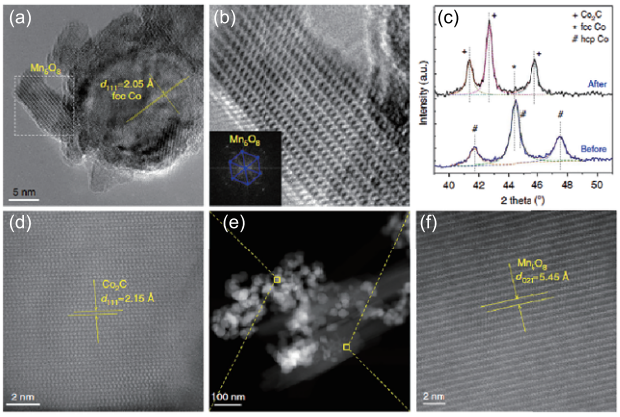

Figure 19 Structural characterization of $Co_4Mn_1K_{0.1}$ catalysts. (a) HRTEM image of $Co_4Mn_1K_{0.1}$ catalyst before reaction; (b) enlarged HRTEM image (inset: the Fourier transform of the selected region of (a)); (c) XRD patterns of $Co_4Mn_1K_{0.1}$ catalyst: both before and after CO hydrogenation; (d–f) HAADF-STEM images of $Co_4Mn_1K_{0.1}$ catalyst after CO hydrogenation [145] (color online).

3.3 Modified Fe-based catalysts

Besides modified Co-based catalysts, the modified Fe-based catalyst systems, especially the Cu-Fe based catalysts with or without promoters, are another kind of HAS catalysts that have been studied widely [105]. The Cu-Fe based catalysts exhibit higher WGS activity and thus making it very suitable for the CO-rich syngas (mainly derived from coal or biomass) conversion. It is clear that Cu, well-known as the major element for methanol synthesis, serves as the dissociative chemisorption of hydrogen and the associative adsorption of CO, while the FeC_x acts as the dissociative CO adsorption and hydrogenation. The synergy between Cu and FeC_x was required for the efficient production of higher alcohols. According to the published results [105], a Cu-Fe catalyst with a homogeneous distribution of the dual sites at an atomic distance would largely improve the HAS performance, while the agglomeration of any site or the separation of the dual sites would result in poor higher alcohol selectivity.

Our group [104,105,146–148] has studied an unsupported CuFe bimetallic nanoparticle for high alcohol synthesis. These catalysts were prepared by simultaneous reduction of cupric and ferric nitrates with sodium borohydride ($NaBH_4$) in ethylene glycol (EG) under Ar atmosphere. The reaction conditions were 200 °C, 60 bar, 6000 h^{-1}, and a H_2/CO of 2. Under these conditions, a Cu/Fe catalyst with a molar ratio of 1/3 exhibited the highest C_{2+}OH and C_{6+}OH selectivity of 95.7 wt% and 74 wt%, respectively, in the total alcohol distribution while maintaining a low methane selectivity at high CO conversion (26%) [146]. In comparison with the Fe nanoparticles and composite nanoparticles of the physical mixture of Fe and Cu nanoparticles, the CuFe bimetallic samples showed comparable CO conversion and similar product distributions, but with much higher selectivity to higher alcohols. The total alcohol selectivity appeared to be more affected by the Cu-FeC_x synergism, while the higher alcohol selectivity depended more on the nature of the FeC_x site. By further investigation of the structural evolution during the reaction process, we found that the Cu and Fe components were homogeneously dispersed and contacted with each other on the nanometer scale at the early stage of the reaction, which contributed to the high total alcohol selectivity due to the good synergism between the dual sites. During the reaction, however, a separation of Cu

and Fe phases was observed, weakening the synergism and decreased the targeted alcohol selectivity (Scheme 3). Thus, we found it very important to increase the concentration of the dual sites on the catalyst surface and maintain the synergism without any phase separation in order to obtain a good HAS performance.

Moreover, the catalytic performance of CuFe, CuCo and CuNi bimetallic catalysts prepared by the same method was studied for comparison under the same reaction conditions [104]. With the aiding of XRD, TEM and EDS characterization technologies, a severe phase separation of Cu and Fe in the spent CuFe samples was observed, and the Cu@Co core-shell structure was formed with the co-existence of the Cu-Co alloy nanoparticles for spent CuCo catalysts, while only Cu-Ni alloys could be observed on the spent CuNi surface. These structural differences resulted in the difference in the catalytic performance. The CuFe catalyst mainly kept the original FT property of Fe, CuCo exhibited different performance from Co, and CuNi acted as a methanol synthesis catalyst rather than higher alcohol or FT synthesis catalyst.

In order to elucidate the reaction network of higher alcohol synthesis over the Cu-Fe based catalysts, the probe molecule experiments (alkane, alcohol, aldehyde and olefin) over the CuFe/ZrO_2 catalyst under the typical HAS reaction conditions was carried out [148]. According to the results, a reaction network was summarized and depicted in Scheme 4. The probe molecular experiments showed that the alkyl intermediates and acyl species formed during the reaction. The alkyl species, formed by CH_2 polymerization, can be hydrogenated to alkanes or converted into acyl species by CO insertion through the synergism of the dual sites. The acyl species can also be terminated to form aldehydes or alcohols by hydrogenation. In addition, the acyl species can react with

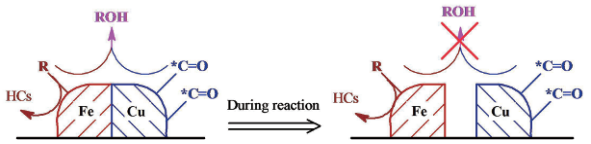

Scheme 3 Schematic depiction of structural evolution of CuFe dual site through the whole reaction: from close contact at the early stage of reaction to phase separation after reaction [147] (color online).

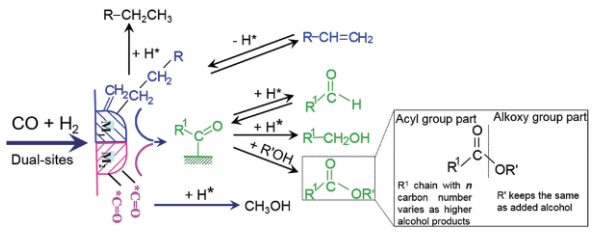

Scheme 4 Schematic illustration of the active site and reaction network over a CuFe catalyst during high alcohol synthesis [148] (color online).

alcohols to form the corresponding esters. This study suggests that the reaction network can be adjusted for high selectivity to the target products by the precise control of both the catalyst and engineering factors.

By optimizing the catalyst preparation method, catalyst composition, pretreatment, and reaction conditions, Xu *et al.* [149] developed an efficient Fe modified CuMnZrO_2 HAS catalyst. The introduction of Fe into the CuMnZrO_2 catalyst by impregnation increased the interaction between the dispersed Cu and Fe compared to co-precipitation, which favors the production of higher alcohols. To further improve the selectivity to alcohols, the Zn promoter was added to the original catalyst resulting in much higher activity and selectivity to alcohols [99]. The corresponding catalyst showed good stability during the 2400 h laboratory test (Figure 20) and was also successfully scaled-up, and passed the single tube reactor test.

Recently, Hou *et al.* [150] prepared the SiO_2-coated CuFe catalysts with different Cu/Fe molar ratios by the co-reduction method and the subsequent *in situ* coating method. The prepared SiO_2-CuFe catalysts were tested at 280 °C, 40 bar, and GHSV of 5000 h^{-1} and a H_2/CO ratio of 2. A Cu/Fe molar ratio of 1 was found to give the highest total alcohol selectivity of 6.5% with a C_{2+} alcohol distribution of 73.9% in the total alcohols, which was caused by a stronger Cu-Fe synergistic effect due to the formation of $CuFe_2O_4$ during the reaction.

Promoters such as Mn, Zr, Ce, and Zn were usually used to modify the Cu-Fe catalyst [151–153]. Han *et al.* [153] studied the Cu-Mg-Fe-M-O (M=Mn,Zr and Ce) catalysts derived from LDH precursors using the co-precipitation method for HAS. The amount of tetrahedrally coordinated Cu species was found to have a liner relationship with the alcohol selectivity. Different promoters have different interaction with the active component leading to varied catalytic performance (Scheme 5). The Mn additive facilitated a stronger interaction between Cu and Fe, and promoted the total alcohol and higher alcohol formation, while the Zr and Ce weakened its interaction with the active component but promoted the interaction of Cu and Fe, and thus resulted in the increased total alcohol selectivity but decreased the C_{2+}OH selectivity.

K has also been used as a chemical promoter to improve the oxygenate selectivity [154]. Many reviews and articles discussed the effect of K addition on the CO hydrogenation activity. K was usually considered to enhance the chemisorption of CO, suppress the chemisorption of H_2, and decrease the reduction degree of the active metal. The excess K would block the active sites and reduce the activity and selectivity of the catalyst, thus a suitable amount of K is advantageous to HAS. Ding *et al.* [154] found a Cu-Fe catalysts with 0.5 wt% K loading to display the highest activity of 27.3% and C_{2+}OH/C_1OH of 1.7 at 260 °C, 40 bar, 6000 h^{-1} of GHSV, and a H_2/CO ratio of 2. Also, K is an effective promoter to

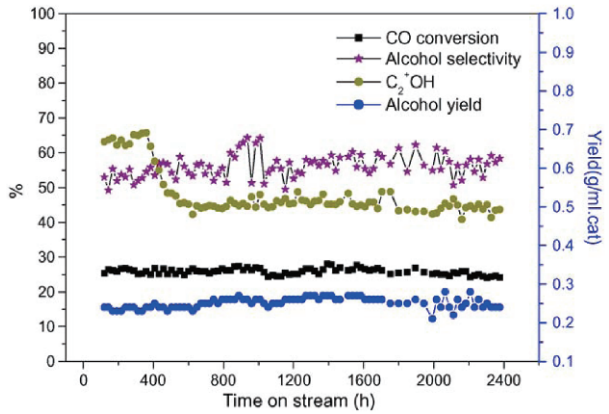

Figure 20 The catalytic performance of Zn promoted FeCu-based catalyst with TOS. Reaction conditions: T=260 °C; P=60 bar; H_2/CO=2.0; GHSV=6000 h^{-1} [99] (color online).

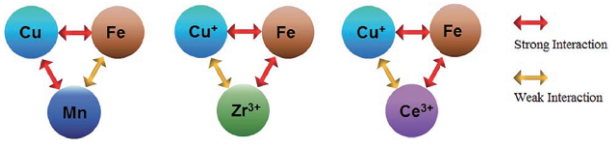

Scheme 5 Schematic depiction of the promoting effects of Mn, Zr and Ce on CuFe catalyst [153] (color online).

suppress CH_4 formation, and shift the product distribution to heavier hydrocarbons.

In addition, a recently published work from Lu *et al.* [155] introduced a three-dimensionally ordered macroporous Cu-Fe catalyst prepared using a glyoxylate route colloidal crystal template method. They tested its HAS performance and observed a very high selectivity to 1-alcohls up to approximately 48% with the distribution of the C_{2+} and C_{6+} slates in total alcohols up to 95% and 63%, respectively. They ascribed this significant breakthrough to unique the macroporous structure of the catalyst and the synergetic effect between the Cu^0 and Fe_5C_2 dual sites.

Other supported iron-based catalyst such as attapulgite [156] and activated palygorskite [157] supported CuFeCo-based catalysts have also been reported. These supporters are added to the Cu-Fe catalyst systems to promote the interaction of the dual sites and stablize the corresponding species.

4 Conclusions and outlook

Production of fuels and chemicals, especially the high value compounds such as lower olefins and higher alcohols, from syngas, will become increasingly important in a world with rising energy consumption and expected depletion of non-renewable petroleum reserves. The direct and highly efficient conversion of syngas into valued-added chemicals is one of the major fields of green carbon science and will become one of the most attracting routes in the near future for lowering the petroleum dependence and realizing the clean utilization of carbon resources. In addition, the growing market demand for the lower olefins and higher alcohols will further drive the research and development in the production processes including the development of catalysts, reactor and related process technology from non-petroleum feedstocks.

As for the direct production of lower olefins via syngas over the dual functional site catalyst systems (for example, OX-ZEO), the reactivity and stability under the industrial conditions should be further improved. Due to the high reaction temperature (~400 °C), coke deposition over zeolite and sintering of the active phase would be the most challenging issues. The selection of supports and proper promoters for the CO-activated component and the tuning of the pore structure and acid properties for the second zeolite component would be future research directions.

Although the FTO process for the lower olefin production does not display higher selectivity towards C_{2-4} olefins than that of MTO, DMTO or OX-ZEO, the chemicals obtained from the FTO process were more flexible and higher value-added. Current progress in the design of active sites, especially the development of Co_2C nanoprisms with exposed facets of (101) and (020), would break the traditional ASF distribution. Lower methane selectivity, higher C_{2-4} olefins selectivity and more stable catalytic performance make it attractive for both the academic and industrial communities. The progress in the FTO process will add fresh momentum to the traditional FTS field. The CO-rich syngas without any H_2/CO adjustment by the water-gas-shift reaction, which has significant energy consumption, can be directly used to synthesize clean targeted products. The FTO process with process simplicity and energy saving will hopefully be industrialized in these coal- or biomass-abundant districts if the following issues are solved: (1) Iron is inexpensive, and the reactivity and selectivity to lower olefins with Fe-based FTO catalysts are rather promising. However, Fe-based FTO catalysts are easy to deactivate due to the coke deposition and particle size growth. In addition, the product distribution of Fe-based FTO catalysts generally follows the ASF model and methane selectivity is still rather high. The catalyst lifetime involving the stability and regeneration property under industrial conditions are the key problems. Thus, the catalytic performance should be further improved by optimization of the catalyst surface structure. (2) The latest reported Co_2C-based FTO catalyst system seems to possess outstanding catalytic performance with product distribution deviates markedly from the classical ASF distribution. However, cobalt is more expensive than iron, and more attention should be paid to the catalyst stability. The following scientific problems need to be further investigated for Co_2C-based FTO catalyst system, i.e, nanoeffects including size effect and facet effect for the Co_2C phase; the stability of this kind of

Co_2C nanoprisms under industrial reaction conditions; regeneration of the Co_2C-based FTO catalyst. *In-situ* studies are also needed to further reveal the structure-performance relationship. In addition, due to the strong exothermicity of the FTO reaction, the reactor engineering should also be further considered. (3) Long-chain olefins are of higher values than lower olefins. For both Fe-based and Co-based FTO catalysts, long chain olefins are also produced. One of the advantages of the FTO process is the tunable property of the product selectivity. It may be more economical to shift the products toward long-chain olefins by optimization of catalyst components and reaction conditions. In the near future, the long-chain olefins will draw more attention due to the current low price of crude oil and flat chemical market.

As for the high alcohols synthesis from syngas, modified FT catalyst systems afford high $C_{2+}OH$ selectivity. However, the activity and stability need to be further improved. Although a consensus has been reached on the bifunctional catalysis for HAS over modified FT catalyst, the information about the detailed dual active sites is still limited. The complexity of the reaction network and the toughness of the reaction conditions in HAS makes the research on the dual active site of actual structure become thorny. The conventional surface characterization methods could not reveal the structural evolution of the HAS catalysts under rigorous reaction conditions. Therefore, researchers need to develop *in-situ* characterization methods and combine the catalytic performance study with in-depth investigation on the structural evolution of HAS catalysts under working conditions. An alternative way might be the design of more elegant experiments to study the structure of the catalysts by existing characterization methods. In addition, strategies to construct and stabilize the dual sites are also very important for HAS studies. More efforts are needed to develop controlled preparation methods to obtain dual active sites with a specific nanostructure. And close attention should be paid to the preparation process since the effect of each step in the preparation might have a significant influence on the performance of the obtained catalyst. Another aspect for the development of the HAS catalysts should be the stabilization of the dual active sites by adding promoters and optimizing the reaction conditions. Moreover, the elucidation of the underlying mechanism and the structure evolution of the dual sites during the reaction are also highly important.

Acknowledgments This work was supported by the National Natural Science Foundation of China (91545112, 21573271, 21403278), Shanghai Municipal Science and Technology Commission, China (15DZ1170500), and the Chinese Academy of Sciences (QYZDB-SSW-SLH035).

Conflict of interest The authors declare that they have no conflict of interest.

1 He M, Sun Y, Han B. *Angew Chem Int Ed*, 2013, 52: 9620–9633
2 Anastas PT, Warner JC. *Green Chemistry: Theory and Practice*. New York: Oxford University Press, 1998
3 Tang SLY, Smith RL, Poliakoff M. *Green Chem*, 2005, 7: 761–762
4 Horváth IT, Anastas PT. *Chem Rev*, 2007, 107: 2169–2173
5 Li CJ, Anastas PT. *Chem Soc Rev*, 2012, 41: 1413
6 Sheldon RA. *Chem Commun*, 2008, 3352
7 Calvo-Flores FG. *ChemSusChem*, 2009, 2: 905–919
8 Tang SY, Bourne RA, Smith RL, Poliakoff M. *Green Chem*, 2008, 10: 268–269
9 Steen EJ, Kang Y, Bokinsky G, Hu Z, Schirmer A, McClure A, Del Cardayre SB, Keasling JD. *Nature*, 2010, 463: 559–562
10 Schilling LB, Landucci R. *FEMS Microbiol Rev*, 1995, 16: 101–110
11 Ren T, Patel MK. *Resour Conserv Recy*, 2009, 53: 513–528
12 Schobert HH, Song C. *Fuel*, 2002, 81: 15–32
13 Khodakov AY, Chu W, Fongarland P. *Chem Rev*, 2007, 107: 1692–1744
14 Demirbaş A. *Energy Conv Manag*, 2001, 42: 1357–1378
15 Saxena RC, Adhikari DK, Goyal HB. *Renew Sust Energ Rev*, 2009, 13: 167–178
16 Binder JB, Raines RT. *J Am Chem Soc*, 2009, 131: 1979–1985
17 Serrano-Ruiz JC, Luque R, Sepúlveda-Escribano A. *Chem Soc Rev*, 2011, 40: 5266–5281
18 Wang H, Gao P, Zhao T, Wei W, Sun Y. *Sci China Chem*, 2015, 58: 79–92
19 Ail SS, Dasappa S. *Renew Sust Energ Rev*, 2016, 58: 267–286
20 Shah M, Dai JJ, Guo QX, Fu Y. *Sci China Chem*, 2015, 58: 1110–1121
21 Cerqueira HS, Caeiro G, Costa L, Ramôa Ribeiro F. *J Mol Catal A-Chem*, 2008, 292: 1–13
22 Corma A, Sauvanaud L, Doskocil E, Yaluris G. *J Catal*, 2011, 279: 183–195
23 Corma A, Melo FV, Sauvanaud L, Ortega F. *Catal Today*, 2005, 107-108: 699–706
24 Torres Galvis HM, de Jong KP. *ACS Catal*, 2013, 3: 2130–2149
25 Tian P, Wei Y, Ye M, Liu Z. *ACS Catal*, 2015, 5: 1922–1938
26 Yu F, Li ZJ, An YL, Gao P, Zhong LS, Sun YH. *J Fuel Chem Technol*, 2016, 44: 801–814
27 Chen JQ, Bozzano A, Glover B, Fuglerud T, Kvisle S. *Catal Today*, 2005, 106: 103–107
28 Dahl IM, Kolboe S. *Catal Lett*, 1993, 20: 329–336
29 Hereijgers BPC, Bleken F, Nilsen MH, Svelle S, Lillerud KP, Bjørgen M, Weckhuysen BM, Olsbye U. *J Catal*, 2009, 264: 77–87
30 Wang W, Jiang Y, Hunger M. *Catal Today*, 2006, 113: 102–114
31 Ying L, Yuan X, Ye M, Cheng Y, Li X, Liu Z. *Chem Eng Res Des*, 2015, 100: 179–191
32 Zhang SC, Yu FC. *Corros Protect Petrochem Ind*, 2016, 33: 5–7
33 La-shan C. *Chem Fertil Design*, 2008, 46: 3–6
34 Olsbye U, Svelle S, Bjørgen M, Beato P, Janssens TVW, Joensen F, Bordiga S, Lillerud KP. *Angew Chem Int Ed*, 2012, 51: 5810–5831
35 Peng X, Cheng K, Kang J, Gu B, Yu X, Zhang Q, Wang Y. *Angew Chem Int Ed*, 2015, 54: 4553–4556
36 Bao J, He J, Zhang Y, Yoneyama Y, Tsubaki N. *Angew Chem*, 2008, 120: 359–362
37 Kang J, Cheng K, Zhang L, Zhang Q, Ding J, Hua W, Lou Y, Zhai Q, Wang Y. *Angew Chem Int Ed*, 2011, 50: 5200–5203
38 Sartipi S, Makkee M, Kapteijn F, Gascon J. *Catal Sci Technol*, 2014, 4: 893–907
39 Ma X, Ge Q, Ma J, Xu H. *Fuel Process Technol*, 2013, 109: 1–6
40 Fujimoto K, Saima H, Tominaga H. *J Catal*, 1985, 94: 16–23
41 Zhang Q, Li X, Asami K, Asaoka S, Fujimoto K. *Fuel Process*

Technol, 2004, 85: 1139–1150
42 de Jong KP. *Science*, 2016, 351: 1030–1031
43 Jiao F, Li J, Pan X, Xiao J, Li H, Ma H, Wei M, Pan Y, Zhou Z, Li M, Miao S, Li J, Zhu Y, Xiao D, He T, Yang J, Qi F, Fu Q, Bao X. *Science*, 2016, 351: 1065–1068
44 Cheng K, Gu B, Liu X, Kang J, Zhang Q, Wang Y. *Angew Chem Int Ed*, 2016, 55: 4725–4728
45 Schulz H. *Appl Catal A-Gen*, 1999, 186: 3–12
46 Zhang R, Liu F, Wang Q, Wang B, Li D. *Appl Catal A-Gen*, 2016, 525: 76–84
47 Fischer FTH. *Brennstoff-Chem*, 1926, 7: 97–104
48 Fischer FTH. *Ber Dtsch Chem Ges*, 1926, 59B: 830–831
49 Okeson TJ, Keyvanloo K, Lawson JS, Argyle MD, Hecker WC. *Catal Today*, 2016, 261: 67–74
50 Brady RC, Pettit R. *J Am Chem Soc*, 1981, 103: 1287–1289
51 Van Der Laan GP, Beenackers AACM. *Catal Rev*, 1999, 41: 255–318
52 Zhang Q, Kang J, Wang Y. *ChemCatChem*, 2010, 2: 1030–1058
53 Koeken ACJ, Torres Galvis HM, Davidian T, Ruitenbeek M, de Jong KP. *Angew Chem Int Ed*, 2012, 51: 7190–7193
54 Dry ME, Erasmus HBW. *Annu Rev Energy*, 1987, 12: 1–21
55 Hu B, Frueh S, Garces HF, Zhang L, Aindow M, Brooks C, Kreidler E, Suib SL. *Appl Catal B-Environ*, 2013, 132–133: 54–61
56 Schulte HJ, Graf B, Xia W, Muhler M. *ChemCatChem*, 2012, 4: 350–355
57 Jiang N, Yang G, Zhang X, Wang L, Shi C, Tsubaki N. *Catal Commun*, 2011, 12: 951–954
58 Iglesia E, Soled SL, Fiato RA. *J Catal*, 1992, 137: 212–224
59 Hadadzadeh H, Mirzaei AA, Morshedi M, Raeisi A, Feyzi M, Rostamizadeh N. *Pet Chem*, 2010, 50: 78–86
60 Bukur DB, Lang X, Mukesh D, Zimmerman WH, Rosynek MP, Li C. *Ind Eng Chem Res*, 1990, 29: 1588–1599
61 Farzad S, Haghtalab A, Rashidi A. *J Energy Chem*, 2013, 22: 573–581
62 Zhang C, Yang Y, Teng B, Li T, Zheng H, Xiang H, Li Y. *J Catal*, 2006, 237: 405–415
63 Bukur DB, Mukesh D, Patel SA. *Ind Eng Chem Res*, 1990, 29: 194–204
64 Sachtler W. *J Catal*, 1985, 92: 429–431
65 Torres Galvis HM, Bitter JH, Khare CB, Ruitenbeek M, Dugulan AI, de Jong KP. *Science*, 2012, 335: 835–838
66 Torres Galvis HM, Koeken ACJ, Bitter JH, Davidian T, Ruitenbeek M, Dugulan AI, de Jong KP. *J Catal*, 2013, 303: 22–30
67 Torres Galvis HM, Bitter JH, Davidian T, Ruitenbeek M, Dugulan AI, de Jong KP. *J Am Chem Soc*, 2012, 134: 16207–16215
68 Oschatz M, Lamme WS, Xie J, Dugulan AI, de Jong KP. *ChemCatChem*, 2016, 8: 2846–2852
69 Xie J, Torres Galvis HM, Koeken ACJ, Kirilin A, Dugulan AI, Ruitenbeek M, de Jong KP. *ACS Catal*, 2016, 6: 4017–4024
70 Zhou X, Ji J, Wang D, Duan X, Qian G, Chen D, Zhou X. *Chem Commun*, 2015, 51: 8853–8856
71 Bussemeier B, Frohning CD, Cornils B. *Hydrocarb Process*, 1976, 56: 105−112
72 Bussemeier B, Frohning CD, Horn G, Kluy W. Process for the production of unsaturated hydro-carbons. US Patent, 4455395, 1984-6-19
73 Venter J. *J Catal*, 1987, 103: 450–465
74 Roy SC, Prasad HL, Dutta P, Bhattacharya A, Singh B, Kumar S, Maharaj S, Kaushik VK, Muthukumaru Pillai S, Ravindranathan M. *Appl Catal A-Gen*, 2001, 220: 153–164
75 Yang Z, Pan X, Wang J, Bao X. *Catal Today*, 2012, 186: 121–127
76 Liu Y, Chen JF, Bao J, Zhang Y. *ACS Catal*, 2015, 5: 3905–3909
77 Huo CF, Li YW, Wang J, Jiao H. *J Am Chem Soc*, 2009, 131: 14713–14721
78 Gao X, Zhang J, Chen N, Ma Q, Fan S, Zhao T, Tsubaki N. *Chin J Catal*, 2016, 37: 510–516
79 Duan X, Wang D, Qian G, Walmsley JC, Holmen A, Chen D, Zhou X. *J Energ Chem*, 2016, 25: 311–317
80 Wang D, Zhou X, Ji J, Duan X, Qian G, Zhou X, Chen D, Yuan W. *J Mater Chem A*, 2015, 3: 4560–4567
81 Xu JD, Zhu KT, Weng XF, Weng WZ, Huang CJ, Wan HL. *Catal Today*, 2013, 215: 86–94
82 Sommen APB, Stoop F, Van Der Wiele K. *Appl Catal*, 1985, 14: 277–288
83 Jones VK, Neubauer LR, Bartholomew CH. *J Phys Chem*, 1986, 90: 4832–4839
84 Zhang JC, Wei GB, Cao WL. *Chin J Catal*, 2003, 24: 259–264
85 Chen X, Deng D, Pan X, Hu Y, Bao X. *Chem Commun*, 2015, 51: 217–220
86 Lu J, Yang L, Xu B, Wu Q, Zhang D, Yuan S, Zhai Y, Wang X, Fan Y, Hu Z. *ACS Catal*, 2014, 4: 613–621
87 Wan H, Wu B, Zhang C, Xiang H, Li Y. *J Mol Catal A-Chem*, 2008, 283: 33–42
88 Zhai P, Xu C, Gao R, Liu X, Li M, Li W, Fu X, Jia C, Xie J, Zhao M, Wang X, Li YW, Zhang Q, Wen XD, Ma D. *Angew Chem Int Ed*, 2016, 55: 9902–9907
89 Tsakoumis NE, Rønning M, Borg Ø, Rytter E, Holmen A. *Catal Today*, 2010, 154: 162–182
90 Fraenkel D, Gates BC. *J Am Chem Soc*, 1980, 102: 2478–2480
91 Mirzaei AA, Faizi M, Habibpour R. *Appl Catal A-Gen*, 2006, 306: 98–107
92 Chen H, Adesina AA. *Appl Catal A-Gen*, 1994, 112: 87–103
93 Feyzi M, Khodaei MM, Shahmoradi J. *Fuel Processing Technol*, 2012, 93: 90–98
94 Das D, Ravichandran G, Chakrabarty DK. *Appl Catal A-Gen*, 1995, 131: 335–345
95 Zhong L, Yu F, An Y, Zhao Y, Sun Y, Li Z, Lin T, Lin Y, Qi X, Dai Y, Gu L, Hu J, Jin S, Shen Q, Wang H. *Nature*, 2016, 538: 84–87
96 Claeys M. *Nature*, 2016, 538: 44–45
97 Herman RG. *Catal Today*, 2000, 55: 233–245
98 Jiao G, Ding Y, Zhu H, Li X, Li J, Lin R, Dong W, Gong L, Pei Y, Lu Y. *Appl Catal A-Gen*, 2009, 364: 137–142
99 Fang K, Li D, Lin M, Xiang M, Wei W, Sun Y. *Catal Today*, 2009, 147: 133–138
100 Slaa JC, van Ommen JG, Ross JRH. *Catal Today*, 1992, 15: 129–148
101 Liu YJ, Zuo ZJ, Liu CB, Li C, Deng X, Huang W. *Fuel Processing Technol*, 2016, 144: 186–190
102 Liu Y, Liu C, Li C, Huang W. *Catal Commun*, 2016, 76: 29–32
103 Sun J, Wan S, Wang F, Lin J, Wang Y. *Ind Eng Chem Res*, 2015, 54: 7841–7851
104 Xiao K, Qi X, Bao Z, Wang X, Zhong L, Fang K, Lin M, Sun Y. *Catal Sci Technol*, 2013, 3: 1591–1602
105 Xiao K, Bao Z, Qi X, Wang X, Zhong L, Fang K, Lin M, Sun Y. *Chin J Catal*, 2013, 34: 116–129
106 Xu XD, Doesburg EBM, Scholten JJF. *Catal Today*, 1987, 2: 125–170
107 Zaman S, Smith KJ. *Catal Rev*, 2012, 54: 41–132
108 Su J, Mao W, Xu XC, Yang Z, Li H, Xu J, Han YF. *AIChE J*, 2014, 60: 1797–1809
109 Anton J, Nebel J, Göbel C, Gabrysch T, Song H, Froese C, Ruland H, Muhler M, Kaluza S. *Top Catal*, 2016, 59: 1361–1370
110 Liu GL, Niu T, Cao A, Geng YX, Zhang Y, Liu Y. *Fuel*, 2016, 176: 1–10
111 Niu T, Liu GL, Chen Y, Yang J, Wu J, Cao Y, Liu Y. *Appl Surface Sci*,

2016, 364: 388–399
112 Zhang R, Liu F, Wang B. *Catal Sci Technol*, 2016, 6: 8036–8054
113 Luk HT, Mondelli C, Ferré DC, Stewart JA, Pérez-Ramírez J. *Chem Soc Rev*, 2017, doi: 10.1039/C6CS00324A
114 Wang Z, Spivey JJ. *Appl Catal A-Gen*, 2015, 507: 75–81
115 Prieto G, Beijer S, Smith ML, He M, Au Y, Wang Z, Bruce DA, de Jong KP, Spivey JJ, de Jongh PE. *Angew Chem Int Ed*, 2014, 53: 6397–6401
116 Volkova GG, Yurieva TM, Plyasova LM, Naumova MI, Zaikovskii VI. *J Mol Catal A-Chem*, 2000, 158: 389–393
117 Xu HY, Chu W, Shi LM, Mang H, Zhou J. *Acta Physico-Chimica Sinica*, 2008, 24: 1085–1089
118 Tien-Thao N, Alamdari H, Zahedi-Niaki MH, Kaliaguine S. *Appl Catal A-Gen*, 2006, 311: 204–212
119 Tien-Thao N, Alamdari H, Kaliaguine S. *J Solid State Chem*, 2008, 181: 2006–2019
120 Gao W, Zhao Y, Chen H, Chen H, Li Y, He S, Zhang Y, Wei M, Evans DG, Duan X. *Green Chem*, 2015, 17: 1525–1534
121 Yang Y, Qi X, Wang X, Lv D, Yu F, Zhong L, Wang H, Sun Y. *Catal Today*, 2016, 270: 101–107
122 Su J, Zhang Z, Fu D, Liu D, Xu XC, Shi B, Wang X, Si R, Jiang Z, Xu J, Han YF. *J Catal*, 2016, 336: 94–106
123 Xiang Y, Chitry V, Kruse N. *Catal Lett*, 2013, 143: 936–941
124 Xiang Y, Barbosa R, Kruse N. *ACS Catal*, 2014, 4: 2792–2800
125 Xiang Y, Chitry V, Liddicoat P, Felfer P, Cairney J, Ringer S, Kruse N. *J Am Chem Soc*, 2013, 135: 7114–7117
126 Xiang Y, Barbosa R, Li X, Kruse N. *ACS Catal*, 2015, 5: 2929–2934
127 Dong X, Liang XL, Li HY, Lin GD, Zhang P, Zhang HB. *Catal Today*, 2009, 147: 158–165
128 Ning X, An Z, He J. *J Catal*, 2016, 340: 236–247
129 Werner S, Johnson GR, Bell AT. *ChemCatChem*, 2014, 6: 2881–2888
130 Du H, Zhu H, Liu T, Zhao Z, Chen X, Dong W, Lu W, Luo W, Ding Y. *Catal Today*, 2017, 281: 549–558
131 Du H, Zhu H, Zhao Z, Dong W, Luo W, Lu W, Jiang M, Liu T, Ding Y. *Appl Catal A-Gen*, 2016, 523: 263–271
132 Gnanamani MK, Jacobs G, Graham UM, Ribeiro MC, Noronha FB, Shafer WD, Davis BH. *Catal Today*, 2016, 261: 40–47
133 Pei Y, Ding Y, Zang J, Song X, Dong W, Zhu H, Wang T, Chen W. *Chin J Catal*, 2015, 36: 252–259
134 Dong WD, Zhu HJ, Ding YJ, Pei YP, Du H, Wang T. *Acta Phys-Chimi Sin*, 2014, 30: 1745–1751
135 Pei YP, Liu JX, Zhao YH, Ding YJ, Liu T, Dong WD, Zhu HJ, Su HY, Yan L, Li JL, Li WX. *ACS Catal*, 2015, 5: 3620–3624
136 de Aquino AD, Gomez Cobo AJ. *Catal Today*, 2001, 65: 209–216
137 Du H, Zhu H, Chen X, Dong W, Lu W, Luo W, Jiang M, Liu T, Ding Y. *Fuel*, 2016, 182: 42–49
138 Bordoloi A, Anton J, Ruland H, Muhler M, Kaluza S. *Catal Sci Technol*, 2015, 5: 3603–3612
139 Shen GC, Liu AM, Shido T, Ichikawa M. *Top Catal*, 1995, 2: 141–154
140 Jiao G, Ding Y, Zhu H, Li X, Dong W, Li J, LÜ Y. *Chin J Catal*, 2009, 30: 92–94
141 Mahdavi V, Peyrovi MH, Islami M, Mehr JY. *Appl Catal A-Gen*, 2005, 281: 259–265
142 Anton J, Nebel J, Song H, Froese C, Weide P, Ruland H, Muhler M, Kaluza S. *J Catal*, 2016, 335: 175–186
143 Wang Z, Kumar N, Spivey JJ. *J Catal*, 2016, 339: 1–8
144 Subramanian ND, Balaji G, Kumar CSSR, Spivey JJ. *Catal Today*, 2009, 147: 100–106
145 Xiang Y, Kruse N. *Nat Commun*, 2016, 7: 13058
146 Xiao K, Bao Z, Qi X, Wang X, Zhong L, Lin M, Fang K, Sun Y. *Catal Commun*, 2013, 40: 154–157
147 Xiao K, Bao Z, Qi X, Wang X, Zhong L, Fang K, Lin M, Sun Y. *J Mol Catal A-Chem*, 2013, 378: 319–325
148 Yang Y, Wang L, Xiao K, Zhao T, Wang H, Zhong L, Sun Y. *Catal Sci Technol*, 2015, 5: 4224–4232
149 Xu R, Yang C, Wei W, Li W, Sun Y, Hu T. *J Mol Catal A-Chem*, 2004, 221: 51–58
150 Hou B, Han X, Lin M, Fang K. *J Fuel Chem Tech*, 2016, 44: 217–224
151 Lu Y, Yu F, Hu J, Liu J. *Appl Catal A-Gen*, 2012, 429-430: 48–58
152 Ding M, Qiu M, Liu J, Li Y, Wang T, Ma L, Wu C. *Fuel*, 2013, 109: 21–27
153 Han X, Fang K, Sun Y. *RSC Adv*, 2015, 5: 51868–51874
154 Ding M, Tu J, Qiu M, Wang T, Ma L, Li Y. *Appl Energ*, 2015, 138: 584–589
155 Lu Y, Cao B, Yu F, Liu J, Bao Z, Gao J. *ChemCatChem*, 2014, 6: 473–478
156 Guo H, Zhang H, Peng F, Yang H, Xiong L, Wang C, Huang C, Chen X, Ma L. *Appl Catal A-Gen*, 2015, 503: 51–61
157 Guo H, Zhang H, Peng F, Yang H, Xiong L, Huang C, Wang C, Chen X, Ma L. *Appl Clay Sci*, 2015, 111: 83–89